

RESEARCH ARTICLE | MAY 13 2024

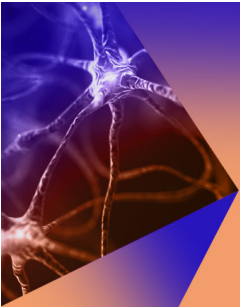
Double harmonic mode-locking in soliton fiber ring laser acquired through the resonant optoacoustic coupling

V. A. Ribenek ; P. A. Itrin ; D. A. Korobko ; A. A. Fotiadi  




APL Photonics 9, 056105 (2024)

<https://doi.org/10.1063/5.0195623>



APL Photonics
Special Topic:
Photonics in Biomedicine

Submit Today



Double harmonic mode-locking in soliton fiber ring laser acquired through the resonant optoacoustic coupling

Cite as: APL Photon. 9, 056105 (2024); doi: 10.1063/5.0195623

Submitted: 3 January 2024 • Accepted: 25 April 2024 •

Published Online: 13 May 2024



View Online



Export Citation



CrossMark

V. A. Ribenek,¹  P. A. Itrin,¹  D. A. Korobko,^{1,a)}  and A. A. Fotiadi^{1,2,b)} 

AFFILIATIONS

¹Ulyanovsk State University, 42 Leo Tolstoy Street, Ulyanovsk 432970, Russian Federation

²Electromagnetism and Telecommunication Department, University of Mons, Mons B-7000, Belgium

^{a)}korobkotam@rambler.ru

^{b)}Author to whom correspondence should be addressed: Andrei.Fotiadi@umons.ac.be

ABSTRACT

Passive harmonic mode-locking of a soliton fiber laser locked to optoacoustic resonance (OAR) in the cavity fiber ensures high-frequency laser operation, high pulse stability, and low timing jitter. However, the pulse repetition rate (PRR) of such lasers is limited to ~ 1 GHz for standard fibers due to the available acoustic modes. Here, we address these limitations by demonstrating a soliton fiber laser built from standard fiber components and subjected to double harmonic mode-locking (DHML). As an example, the laser adjusted to operate at the 15th harmonic of its cavity matching the OAR at ~ 199 MHz could be driven to operate at a high harmonic of this particular OAR frequency, thus reaching ~ 12 GHz. This breakthrough is made possible through controllable optoacoustic interactions in a short, 50 cm segment of unjacketed cavity fiber. We propose that the precise alignment of the laser cavity harmonic and fiber acoustic modes leads to a long-lived narrow-band acoustic vibration. This vibration sets the pace for the pulses circulating in the cavity by suppressing modes that do not conform to the Vernier principle. The surviving modes, equally spaced by the OAR frequency, in cooperation with the gain depletion and recovery mechanism, facilitate the formation of stable high-frequency pulse sequences, enabling DHML. In this process, the OAR rather than the laser cavity defines the elementary step for laser PRR tuning. Throughout the entire PRR tuning range, the soliton fiber laser exhibits enhanced stability, demonstrating supermode suppression levels better than ~ 40 dB and picosecond pulse timing jitter.

© 2024 Author(s). All article content, except where otherwise noted, is licensed under a Creative Commons Attribution (CC BY) license (<https://creativecommons.org/licenses/by/4.0/>). <https://doi.org/10.1063/5.0195623>

I. INTRODUCTION

High repetition rate operation of low-noise ultrafast lasers is crucial for their various applications, such as optical fiber telecommunications, microwave photonics, frequency metrology, and high-speed optical processing.^{1–4} Passively mode-locked fiber lasers are particularly attractive due to their simple design, wavelength tunability, and sub-picosecond operation.^{5–8} However, these lasers usually support a single pulse circulating inside the laser cavity, producing a pulse repetition rate (PRR) equal to the cavity's round-trip frequency, f_0 . Given the considerable length of the fiber laser cavity, the fundamental PRR typically ranges from tens to hundreds of MHz, thus limiting the areas of their potential applications.

Harmonic mode-locking (HML) offers a method that is less technically challenging and more convenient to increase the available PRR of pulsed lasers by supporting multiple, uniformly spaced pulses within the cavity. In the soliton fiber laser configuration, HML operation can be achieved due to physical mechanisms that enhance mutual repulsion between the pulses, enabling a uniform pulse arrangement over the cavity. These mechanisms are needed to counteract the laser noise, which continuously perturbs the pulses, disrupting their equidistant spacing. Several mechanisms ensure pulse repulsion, including interactions mediated by gain depletion and recovery (GDR) processes,^{9–12} interactions provided by the guided acoustic wave Brillouin scattering (GAWBS),^{13–16} and interactions transmitted through dispersion waves or continuous waves

co-propagating the pulses in the laser cavity.^{17–20} However, since these interactions are typically weak, the temporal jitter (i.e., fluctuations of inter-pulse intervals) in HML lasers is high compared to that in lasers operating fundamental mode-locking.²¹

To achieve stable laser operation in the HML regime, one can utilize effects that are resonantly enhanced to assist in maintaining equidistant soliton spacing in the laser cavity.^{22–29} Specifically, the laser can include an additional high Q resonator with a free spectral range (FSR) equal to an integer multiple of the laser cavity's round-trip frequency.^{30–32} Although such a configuration can produce stable pulses with a PRR equal to the FSR of the additional resonator, the need for complex electronic systems to control the phase difference between the laser cavity and the additional resonator complicates the system and reduces its practicality. A similar HML operation is achievable in an active fiber laser configuration that includes a phase or amplitude modulator driven in resonance with one of the laser cavity harmonics.³³

However, the simplest way to stabilize the soliton laser to a high frequency is to use the natural GAWBS resonances governed by the radial (R_{0m}) or torsional-radial (TR_{2m}) acoustic modes in the cavity fiber.^{34–36} In this approach, the high-frequency pulse train, propagating in the cavity fiber, drives a trapped acoustic wave through electrostriction. In turn, the index modulation produced by the vibration acts on the driving pulses. The enhanced optoacoustic resonance (OAR) in the fiber core allows successive pulses to interact, efficiently stabilizing the pulse spacing in the fiber laser cavity and suppressing pulse timing jitter. This technique has been applied to the soliton laser constructed from a photonic crystal fiber with acoustic resonances in the gigahertz domain to demonstrate stable harmonic mode-locking at ~ 2.5 GHz.^{36–39} However, in conventional optical fibers, the R_{0m} and TR_{2m} acoustic modes activate at frequencies below 500 MHz and 1 GHz, respectively, limiting the PRR range achievable with standard fiber lasers.^{40–44}

In this paper, we introduce a method enforcing the soliton fiber ring laser to generate a stable gigahertz pulse train. The laser operation mechanism involves OAR in the standard cavity fiber, but unlike previously reported techniques, it does not limit the range of available PRR. To implement this operation, the soliton fiber laser is precisely adjusted to ensure one of the laser cavity harmonics coincides with the selected radial (R_{0m}) or torsional-radial (TR_{2m}) mode. After self-starting, the laser operates this selected laser harmonic, resulting in the generation of a robust pulse sequence with a supermode suppression level (SSL) of over 60 dB and excellent long-term

stability. What is surprising is that such preadjusted laser configuration can be further used with higher pump powers to generate different harmonics of the selected OAR frequency enabling stable pulse trains with deeply suppressed supermode noise. In particular, we demonstrate an Er-doped HML fiber laser adjusted for the resonance between its 15th harmonic and TR_{09} cavity fiber GAWBS mode at $f_a \sim 199$ MHz but operating stable pulse sequences with the PRR exceeding ~ 12 GHz. The controllable PRR tuning could occur in either a positive or negative direction with an elementary step equal to the selected OAR frequency, f_{res} . Throughout the entire PRR range, the generated pulses are characterized by the SSL better than ~ 25 dB and picosecond pulse timing jitter.

II. EXPERIMENTAL SETUP AND ARRANGEMENT

The experimental configuration of an Er-doped soliton nonlinear polarization evolution (NPE) mode-locked fiber ring laser is shown in Fig. 1. A unidirectional laser cavity consists of two types of fibers: a 0.8 m long heavily erbium-doped fiber (EDF) with normal dispersion [-48 (ps/nm)/km] and a standard single mode fiber (G.652.D, Fujikura) with anomalous dispersion [17 (ps/nm)/km]. The 15 m long laser cavity determines a fundamental laser frequency of $f_0 = 13.27$ MHz. A fiber isolator (ISO) and in-line polarizer supplied by PM output fibers (~ 0.5 m), two 980/1550 WDM couplers, three paddle fiber polarization controller (PC), and a 5% output coupler (OC) incorporate the fiber birefringence filter into the cavity to realize a fast saturable absorber. The laser is pumped at 980 nm from two laser diodes specified for a maximum power of 550 mW. The central wavelength of the soliton laser can be tuned simply by adjusting the PC that controls the linear birefringence filter formed in the cavity fiber. The laser could be tuned to the wavelengths selected from bands between 1550 and 1590 nm specific for the built fiber configuration. The laser operation is monitored by an optical spectrum analyzer (Yokogawa 6370D) with a resolution of ~ 0.02 nm, a radiofrequency spectrum analyzer (R&S FSP40), and a ~ 4 GHz digital oscilloscope (Keysight) both coupled with a 30 GHz photodetector. The cavity is placed in a foam box to reduce the influence of the lab environment. To enhance the optomechanical effect, the polymer coating has been removed from a 50 cm segment of a single-mode cavity fiber, making the GAWBS resonances narrower and more pronounced.⁴⁰ Specifically, it was fixed between two holders in the laser setup and subjected to mechanical stretching using a pair of mechanical translation stages.

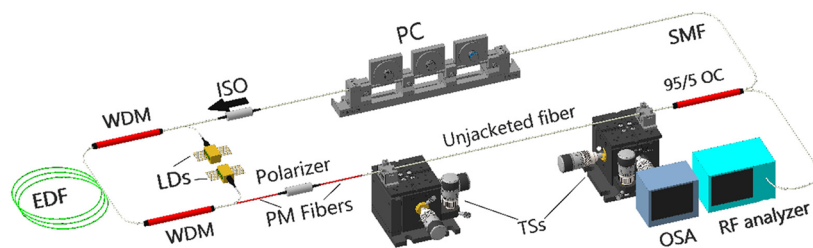


FIG. 1. Experimental setup of the soliton NPE laser. EDF: erbium-doped fiber; WDM: wavelength division multiplexer; LDs: pump laser diodes; SMF: single-mode optical fiber; PM fibers: polarization maintaining optical fibers; ISO: optical fiber isolator; OC: optical coupler; PC: polarization controller; TSs: translation stages; RF analyzer: radio-frequency spectrum analyzer; OSA: optical spectrum analyzer.

A separate experiment was conducted to evaluate the eigenfrequencies of R_{0m} and TR_{2m} acoustic modes in G.652.D (Fujikura) fiber similar to that used in the laser cavity. In the setup shown in Fig. 2(a), linearly polarized radiation from a narrow-band laser (TeraXion Inc.) is amplified by an erbium-doped fiber amplifier (EDFA), passed through an optical isolator (ISO) and an in-line polarization controller (PC1), and then, is launched into a single-mode optical fiber under test. For the detection of depolarized GAWBS modes, PC1 aligns the laser polarization with one of the fiber's extrinsic birefringent axes, and PC2 at the fiber output is adjusted to minimize the optical power transmitted through the optical polarizer (POL) to the pin photodiode (PD).⁴⁵ With PC1 and PC2 correctly adjusted, the PD detects only a small fraction of the GAWBS light, serving as a local oscillator to beat with the signal scattered into the

orthogonal polarization by the depolarized GAWBS modes. The PD signal, recorded by an electrical spectrum analyzer (R&S FSP40), reproduces the GAWBS spectrum. It is noteworthy that the polarized (R_{0m}) GAWBS modes are paired with the TR_{2m} modes sharing the same peak. Therefore, the measurement setup primarily optimized for detecting depolarized (TR_{2m}) modes is able to detect the position of the polarized (R_{0m}) modes as well. A particular challenge is the identification of the exact mode order for each resonance. However, the resonance positions largely depend on the cladding diameter of the SMF structure. This dependency ensures that resonant frequencies determined with telecom optical fibers in various studies—despite employing diverse methodologies—align with remarkable precision. The consistency between experimental the GAWBS mode spectra and their theoretical predictions

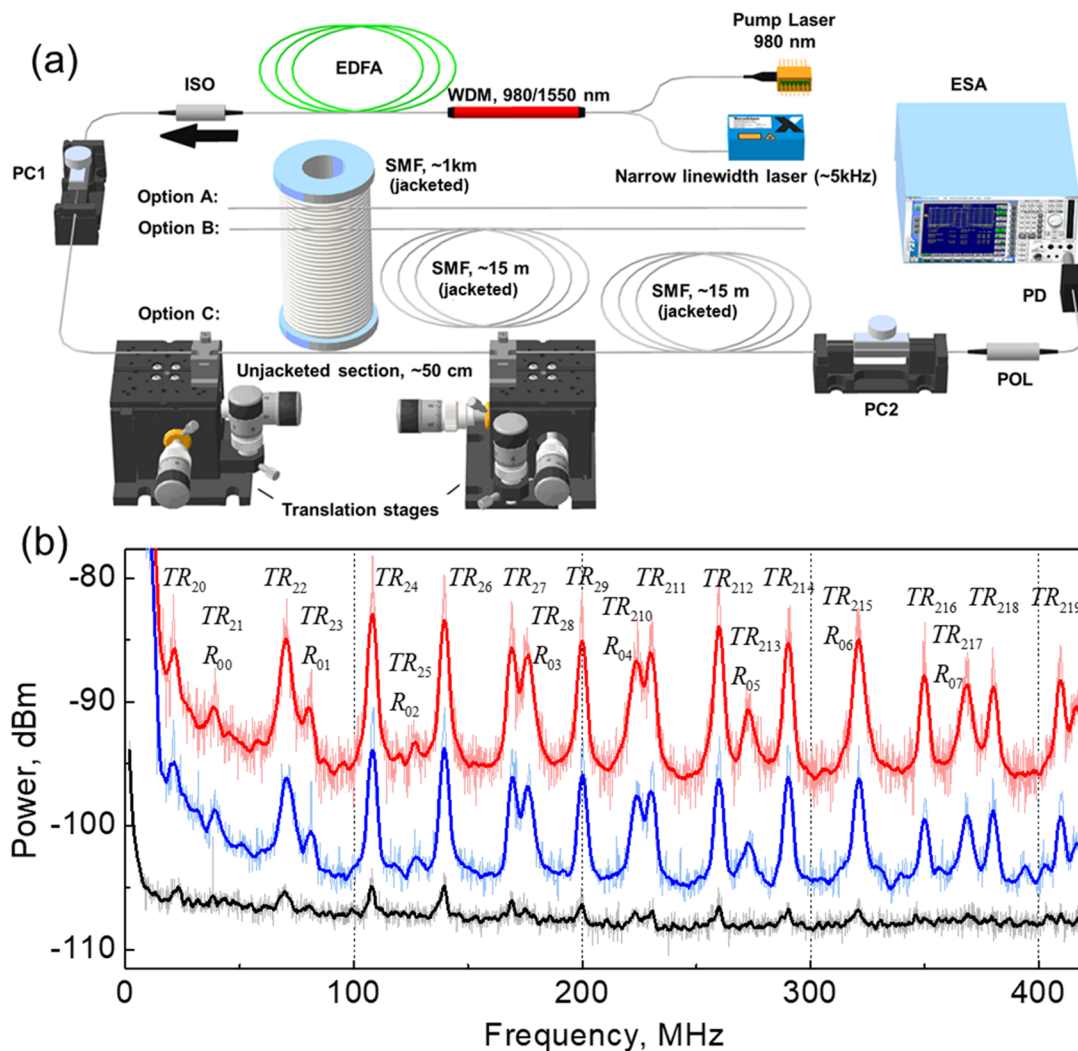


FIG. 2. Experimental setup for GAWBS mode measurements (a) and GAWBS spectra recorded with three samples of the G.652.D fiber (Fujikura) (b). The lengths of the tested samples are as follows: 1 km polymer-coated fiber (option A, red curve), 15 m polymer-coated fiber (option B, black curve), and 15 m polymer-coated fiber incorporating a 50 cm long segment of unjacketed fiber (option C, blue curve).

TABLE I. Measured frequencies of R_{0m} and TR_{2m} GAWBS modes in G.652.D Fujikura optical fiber. Boldface denotes the OAR mode frequency used with the results reported hereafter.

Acoustic mode	TR_{20}	R_{00} (TR_{21})	TR_{22}	R_{01} (TR_{23})	TR_{24}
Frequency, MHz	21.5	38.7	70.06	81.2	107.73
Acoustic mode	R_{02} (TR_{25})	TR_{26}	TR_{27}	R_{03} (TR_{28})	TR_{29}
Frequency, MHz	126.50	138.52	167.97	175.14	198.79
Acoustic mode	R_{04} (TR_{210})	TR_{211}	TR_{212}	R_{05} (TR_{213})	TR_{214}
Frequency, MHz	222.9	229.27	258.33	270.67	288.98
Acoustic mode	R_{06} (TR_{215})	TR_{216}	R_{07} (TR_{217})	TR_{218}	TR_{219}
Frequency, MHz	320.02	347.89	366.99	378.93	407.59

simplifies the task of confirming the exact mode order for each resonance.

The evaluation involved testing three distinct fiber segments, with the results shown in Fig. 2(b). The initial test utilized a 1 km long polymer-coated fiber Option A, red curve), leveraging the long fiber’s capacity to ensure a high signal-to-noise ratio crucial for accurately determining the frequencies of all R_{0m} and TR_{2m} acoustic modes across the spectrum. One can see that the acoustic modes predominantly appeared as discrete, distinctly separated peaks. To precisely assign an exact mode order to each GAWBS resonance, the experimentally recorded GAWBS spectrum was compared to its calculated counterpart in Ref. 42. The frequencies of the GAWBS modes that are identified in this manner are presented in Table I.

The additional spectra shown in Fig. 2(b) were acquired under identical laser power conditions but with a 15 m long polymer-coated fiber (option B, black curve) and a 15 m long polymer-coated fiber incorporating a 50 cm unjacketed segment (option C, blue curve), respectively. The analysis revealed that while the polymer fiber jacket’s presence or absence did not modify the GAWBS mode frequencies, it significantly influenced the resonance peaks’ characteristics. A comparative analysis of the spectra revealed that the unjacketed fiber segment’s contribution to the GAWBS spectrum was tenfold that of the remaining ~15 m of jacketed SMF. This disparity stems from the polymer jacket’s dampening effect on acoustic vibrations within the silica fiber, thereby broadening the

GAWBS resonance linewidth. Figure 3(a) shows a single GAWBS mode spectral peak at 199 MHz (TR_{29}) measured with utmost precision in the 15 m long fiber with the 50 cm unjacketed fiber segment. The peak exhibits a remarkably narrow linewidth of $\Delta f_a \sim 80$ kHz, which is rather typical for unjacketed telecom fibers (for comparison, see Refs. 46–48). In addition, the experiment entailed securing the unjacketed fiber segment between the two holders and subjecting it to mechanical stretching via mechanical translation stages. As it is shown in the inset [Fig. 3(a)], this approach enabled the gradual tuning of the GAWBS resonant frequency (TR_{29}) across a span of ~0.4 MHz with a tuning rate of 0.27 MHz/mm.

Similar stretching techniques have been applied to the 50 cm unjacketed cavity fiber section immediately within the fiber laser cavity, as shown in Fig. 1. To integrate optoacoustic resonance (OAR) into the laser cavity, it is necessary to align a suitable acoustic mode (R_{0m} or TR_{2m}) at f_a with a laser harmonic at $f_{res} = N_{res}f_0$. For this purpose, the laser cavity length is preadjusted so that both frequencies nearly coincide $f_{res} = f_a$. With a perfectly arranged laser configuration, the gradual stretching of the unjacketed fiber segment within the fiber cavity enables tuning of the frequency offset $\delta = (f_{res} - f_a)/\Delta f_a < 0$ between the selected laser cavity harmonic and acoustic mode frequencies across a range of [0, -5], thus enabling precise control of the OAR strength. It is critical to note that without such precision adjustment, the OAR could not be commonly achieved due to the narrow OAR linewidth. The narrow

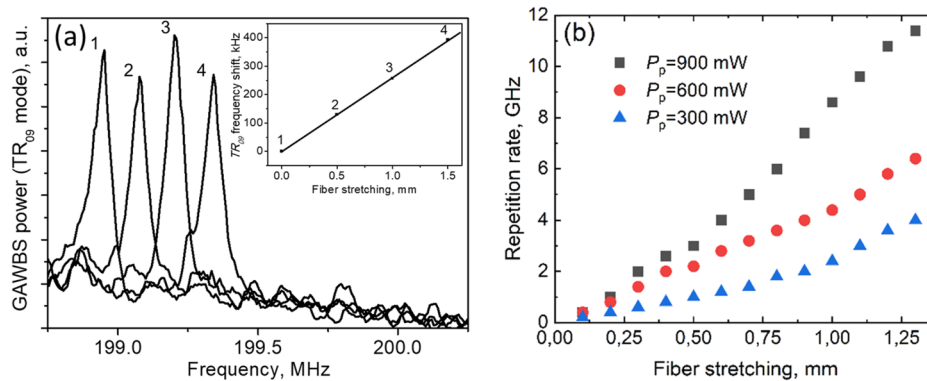


FIG. 3. TR_{29} mode spectra (in linear scale) measured with a 15 m polymer-coated fiber comprising a 50 cm unjacketed fiber segment subjected to stretching (a). Effect of the fiber segment stretching on the PRR of the laser operation in the DHML regime achievable at different pump power levels (b). The inset shows the TR_{29} mode frequency shift induced by the fiber segment stretching; points 1–4 correspond to the measured spectra.

linewidth of OAR plays a crucial role in the specific laser operation regime reported hereafter. We have verified experimentally that a similar stretching applied to a 50 cm long polymer-coated (jacketed) fiber section within the laser cavity has a negligible effect on the laser behavior.

With the aim to provide a clear experimental insight into the laser operation mechanisms, we have compared the performance of an Er-doped soliton NPE mode-locked fiber ring laser without and with its precise adjustment to the OAR. In the first case, the laser operates in a traditional HML manner, whereas in the second case, the laser exhibits pronounced specific features highlighting a new operation regime referred to here as double HML (DHML). We have checked experimentally that DHML is achievable with any GAWBS mode presented in Table I. Nevertheless, the selection of isolated (unpaired) modes, such as TR_{24} , TR_{26} , TR_{29} , and TR_{212} is favored for achieving a more stable DHML operation. In the discussed experiments, the laser cavity length is perfectly matched to the 15th laser harmonic at $f_{res} = 15 \times 13.266$ MHz with the TR_{29} acoustic mode at $f_a = 199$ MHz, ensuring that no other acoustic mode aligns with any laser harmonic.

III. EXPERIMENTAL RESULTS

Our experiments reveal the properties of laser operation at $\lambda \sim 1565$ nm. After the laser is switched on, the desired operation regime could be achieved by precise adjustments of the pump power

level and PC. The mode-locked laser operation is established at a pump power of ~ 80 mW. With the pump power in the range of ~ 80 – 120 mW, the laser still generates regular pulses with the fundamental PRR enabling one soliton circulating in the laser cavity. With a further pump power increase, the laser switches to multi-pulse operation. Accurate manipulations with the PC at this stage allow equalizing the distribution of the pulses over the cavity, thus enabling the traditional HML regime. In the HML regime, the laser emits regular pulses with the PRR corresponding to N pulses per cavity round trip. An increase or decrease in the pump power allows us to change the order of laser harmonic operation commonly one-by-one, resulting in the corresponding changes of the PRR. When the number of the laser operation harmonic gets $N_{res} = 15$, the laser may be subjected to fine-tuning (through the cavity fiber segment stretching) to force its operation in DHML regime. The laser properly adjusted for this operation gets the PRR equal to $f_{res} = N_{res}f_0$ immediately after it is switched on bypassing the intermediate stages. For further PRR switching in the DHML laser, one can use the pump power control or/and PC alignment. The accuracy of the OAR setting, however, determines the maximum achievable PRR value. Figure 3(b) shows the maximal PRRs attainable with the DHML laser at a few pump power levels. With the perfectly adjusted OAR, the PRR tunability is extended up to ~ 12 GHz and can be provided by the pump power control only. Such precise DHML laser presetting has been used in the experiments reported hereafter.

Figure 4(a) compares the PRRs available with the laser operating in the HML and DHML regimes. In both the cases, the PRR changes step-wise. At low pump powers < 270 mW, both PRR curves

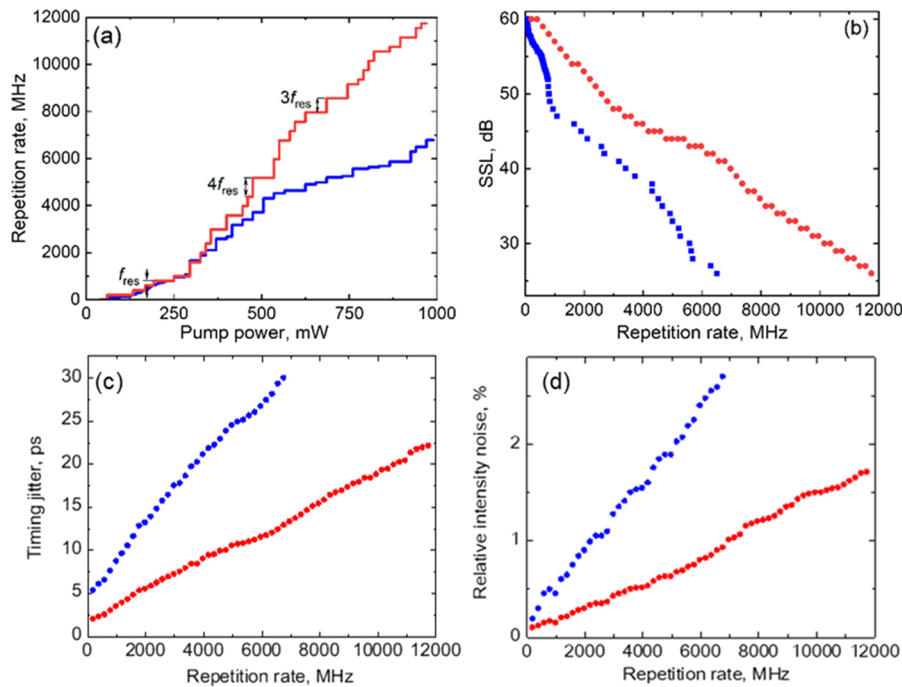


FIG. 4. PRR as a function of the increasing pump power (a) and the SSL (b), timing jitter (c), and RIN (d) as functions of the PRR measured with the soliton laser operating in traditional HML (blue) and DHML (red) regimes.

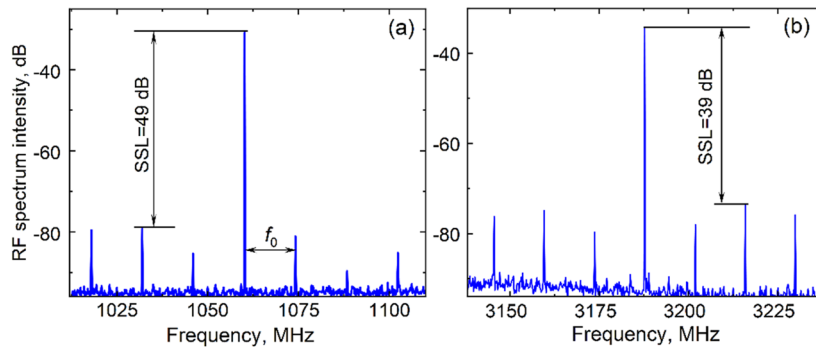


FIG. 5. Typical RF spectra measured with the soliton fiber laser operating in the HML regime with different PRR: $PRR = 80f_0 = 1062$ MHz (a) and $240f_0 = 3185$ MHz (b). The spectral resolution is 200 kHz.

are close to each other possessing the same slope. However, above this point, the curves diverge and keep arising independently until all available pump power is expired. As a result, the PRR of ~ 11.74 GHz, achieved with the DHML laser operation, occurs to be almost two times higher than the PRR of ~ 6.789 GHz reached in the traditional HML regime. Another difference concerns the step of the available PRR changes. For HML laser operation, the elementary PRR step is equal to the fundamental laser frequency f_0 . Indeed, at low pump powers (<270 mW), the pulses in the fiber appear one by one. With a further pump power increase, the PRR increment changes randomly with a step corresponding to the simultaneous appearance of 1–6 pulses in the cavity. Such PRR dynamics is typical

for the HML laser operation.⁴⁹ In contrast to the HML laser operation, the elementary PRR step for the DHML operation is equal to the OAR frequency f_{res} , that is, 15 times the fundamental laser frequency f_0 . Similarly, at low pump powers (<270 mW) the pulses in the laser cavity appear 15 by 15, but with a further pump power increase, the PRR increment could change with a step corresponding to the simultaneous appearance of 15, 30, 45, or 60 pulses in the cavity. To the best of our knowledge, such PRR behavior has not yet been observed with the soliton fiber lasers. It is worth noting that the curves describing the negative PRR changes are similar to those shown in Fig. 4(a) but do not precisely coincide with them due to hysteresis.⁵⁰

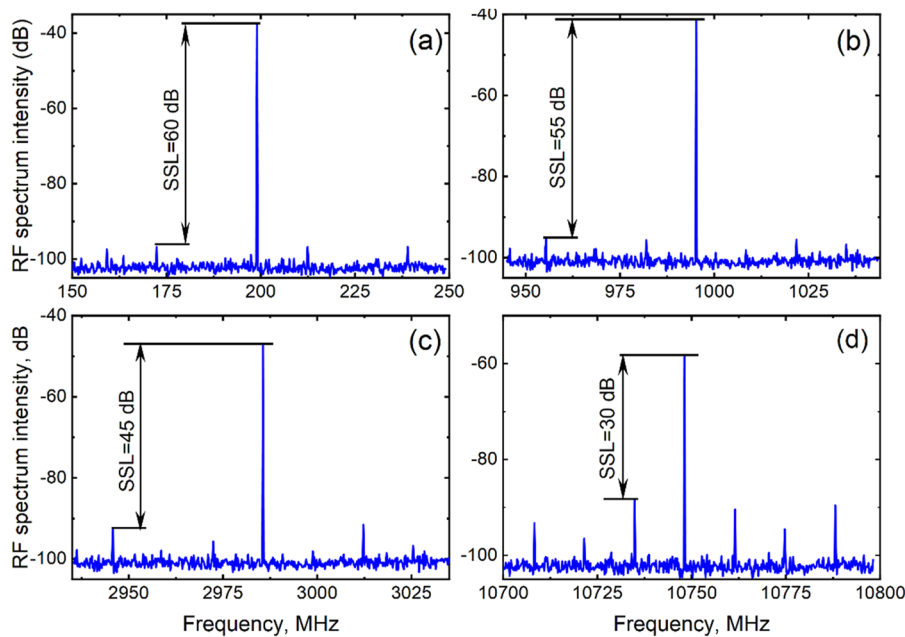


FIG. 6. Typical RF spectra measured with the soliton fiber laser operating in the DHML regime with different PRR: $PRR = f_{res} = 15f_0 = 199$ MHz (a), $5f_{res} = 75f_0 = 995$ MHz (b), $15f_{res} = 225f_0 = 2986$ MHz (c), and $54f_{res} = 810f_0 = 10\,746$ MHz (d). The spectral resolution is 200 kHz.

The difference between the laser operation in steady-state HML and DHML regimes is also pronounced in the RF laser spectra. In the experiments, such spectra are used for advanced monitoring of the soliton laser PRRs and quantitative evaluation of the laser noise. Typical RF spectra recorded with laser operating in the HML regime are shown in Fig. 5. The RF spectrum comprises the main prominent peaks and many small peaks surrounding them. The main peaks are spaced by the current laser PRR, whereas the surrounding small peaks (supermodes) are spaced by the fundamental laser frequency f_0 . A difference between the main peak amplitude and the maximal amplitude of the surrounding supermodes in dB is referred to as the supermode noise suppression level (SSL). It is a crucial HML laser parameter characterizing the periodicity of pulse generation. The integral intensity accumulated in the supermode peaks evaluates the laser pulse jitter, i.e., the fluctuations of pulse amplitudes and inter-pulse intervals in the emitted pulse train.⁵¹ The RF spectra shown in Fig. 5 highlight the SSL of ~30–50 dB measured for the HML laser operating within the PRR range of 0.5–3.5 GHz. For lower PRR, the SSL is higher. For example, Fig. 5(a) estimates the SSL of

~49 dB measured for 1062 MHz. For the PRRs higher than ~2 GHz, the SSL is relatively low, e.g., ~39 dB for 3185 MHz [Fig. 5(b)]. All the measured SSL values are typical for the soliton lasers operating HML with moderate stability and are in agreement with similar experiments reported earlier.^{18,20,24}

The RF spectra recorded with the soliton laser operating in a steady-state DHML regime are shown in Fig. 6. The principal spectrum structure is similar to that shown in Fig. 5, except that the attainable PRRs are harmonics of the OAR frequency. The main prominent peaks with spacing equal to the current laser PRR are surrounded by supermodes with amplitudes much lower than that shown in Fig. 5. At low harmonics, the supermodes are not even resolvable in the RF spectra, meaning that their amplitudes are at least relatively suppressed by 60 dB to the observed peaks. Correspondingly, the suppressed supermodes determine the enhanced SSL and reduced pulse timing jitter restored from the measured RF spectra. For example, the RF spectra shown in Fig. 6 reveal the SSL ~60 dB recorded for the PRR equal to the OAR frequency and comparable SSL values for the PRRs equal to the multiple integers of

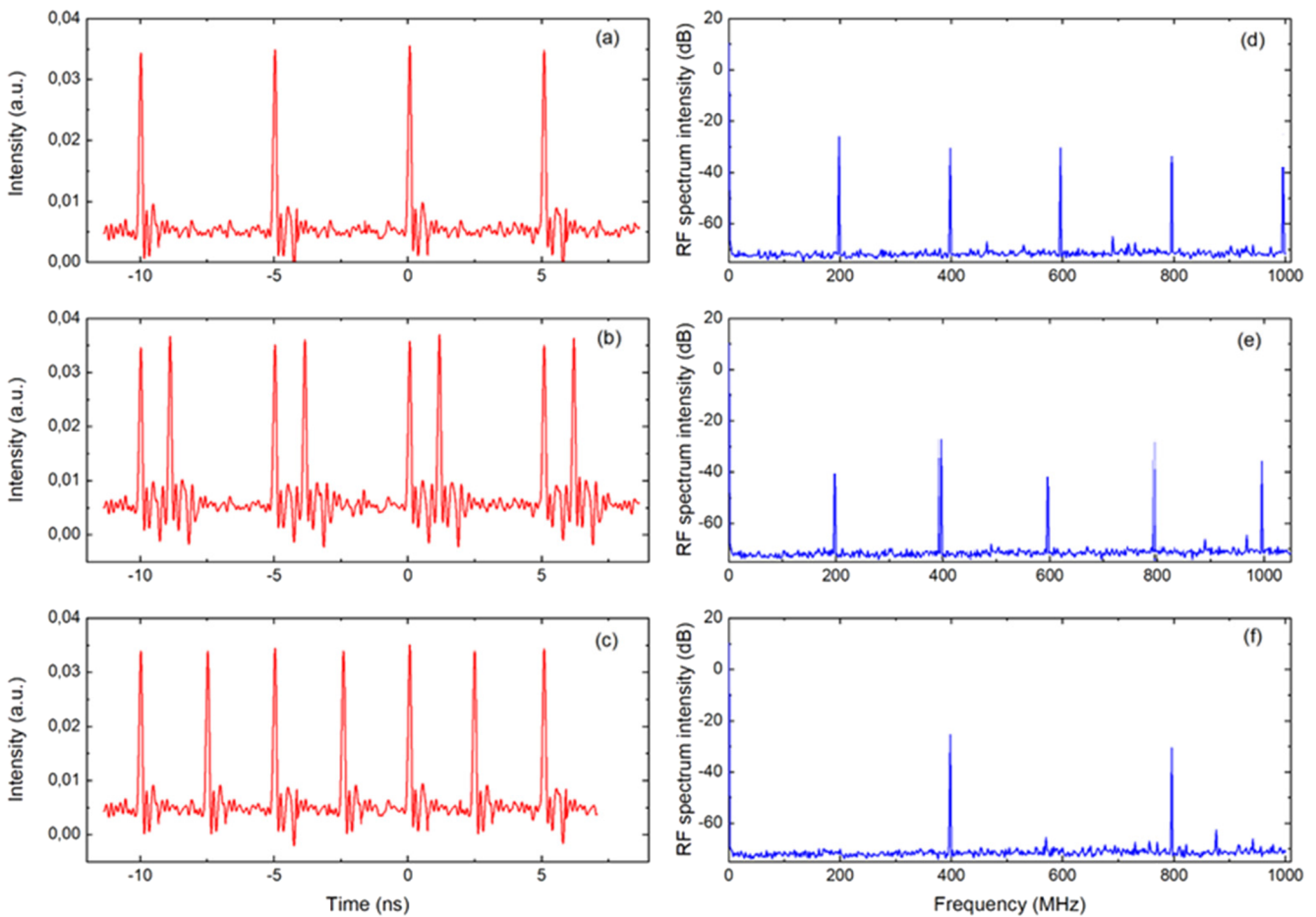


FIG. 7. Typical oscilloscope traces and corresponding RF spectra measured with the DHML laser operating in the initial (a), intermediate (b), and final (c) steady-state regimes during its transition from $PRR = f_{res} = 199$ MHz to $PRR = 2f_{res} = 398$ MHz.

the OAR frequency, thus highlighting the stabilizing effect of the OAR extended to the soliton laser operating the regular pulses at harmonics of the OAR frequency.

The SSL values measured for the laser operating under steady-state HML and DHML regimes are compared, as shown in Fig. 4(b). The measurements were conducted across the entire range of available PRRs, which is twice broader for the DHML operation. Generally, transitioning to DHML operation enhances the stability of the HML laser, resulting in an increase in SSL of $\sim 5\text{--}30$ dB. This enhancement aligns well with the observed improvements in timing jitter and relative intensity noise (RIN), which were measured using a high-speed digital oscilloscope and its built-in statistical functions (standard deviation of the time interval between the nearest pulses and pulse amplitude, respectively). These improvements are shown in Figs. 4(c) and 4(d), respectively, for comparable PRR settings. Notably, the timing jitter decreases by 60% across this range, for instance, dropping from about 17.8 to 7.5 ps when the laser operates with a $PRR = 3184$ MHz in HML and DHML regimes, respectively. Similarly, in terms of RIN, the DHML-operating laser exhibits a remarkable improvement of $\sim 65\%$ compared to its HML operation. To illustrate, at the same $PRR = 3184$ MHz, the RIN diminishes from 1.35% to 0.45%.

Several experiments have been performed to reveal the transition of the DHML operation from one PRR to another. Simultaneous recording of the oscilloscope traces and RF spectra allows monitoring intermediate states of this process. In the experiment shown in Fig. 7, the laser is initially set to operate at $f_{res} = 199$ MHz [Figs. 7(a) and 7(d)]. With a delicate pump power increase, each pulse of the original pulse sequence splits into two pulses and the laser continues to generate a sequence of the pulse doublets

[Fig. 7(b)] keeping the same PRR. In this regime, the pulse sequence can be thought of as a robust superposition of two replicas of the initial sequence separated by a gap of $\Delta T \sim 1$ ns (Visualization 1). In the corresponding RF spectrum [Fig. 7(e)], the main spectral peaks spaced by f_{res} are modulated, with the frequency period determined by the gap as $\sim 1/\Delta T$. At this stage, using an accurate PC adjustment, the gap ΔT between pulses in the doublets could be tuned, enabling the generation of doublet sequences with a given inter-pulse gap ΔT . In particular, the gap can be adjusted to be a half of the pulse period $\Delta T = 1/2f_{res}$ resulting in the suppression of each second peak in the laser RF spectrum thus getting the laser DHML operation with the doubled $PRR = 2f_{res}$ [Figs. 7(c) and 7(f)]. Alternatively, the system transition to the doubled PRR operation could only be completed using a pump power control (Visualization 2).

Similar manipulations can be applied to the laser operating multiple pulses at higher frequencies. In an intermediate state, the laser operates $M \cdot N_{res}$ pulses in the cavity, where M is an integer and $N_{res} = 15$. At any moment, the system maintains the fixed period $T_{res} = 1/f_{res}$ of the pulse distribution over the cavity, i.e., the resulting pulse sequence is always a superposition of M elementary pulse sequences, each comprising $N_{res} = 15$ pulses evenly distributed over the cavity length. The elementary pulse sequences make relative precessions, as illustrated in the accompanying Visualization 3. Its RF spectrum has a rather specific structure, revealing the role of the OAR at $f_{res} = 199$ MHz in the stabilization of the DHML. In contrast to the DHML laser RF spectra [Figs. 8(a), 8(c), 8(d), and 8(f)], the RF spectra of the laser operating in the intermediate state [Figs. 8(b) and 8(e)] exhibit both a pronounced peak at the OAR frequency f_{res} and several supermodes spaced by f_{res} surrounding its principal peak at the current PRR. At the same time, the supermodes with spacing

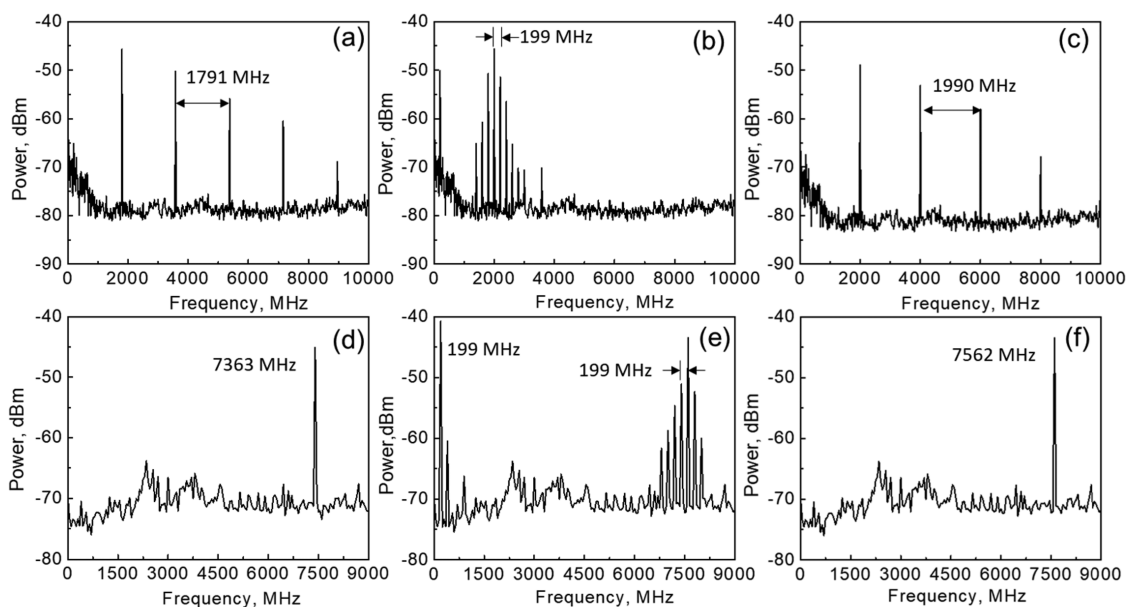


FIG. 8. Typical RF spectra measured with the DHML laser operating in the initial (a) and (d), intermediate (b) and (e), and final (c) and (f) steady-state regimes during its transition from $PRR = 9f_{res} = 135f_0 = 1791$ MHz to $PRR = 10f_{res} = 150f_0 = 1990$ MHz (a)–(c) and $PRR = 37f_{res} = 555f_0 = 7363$ MHz to $PRR = 38f_{res} = 570f_0 = 7562$ MHz (d)–(f). The spectral resolution is 50 MHz.

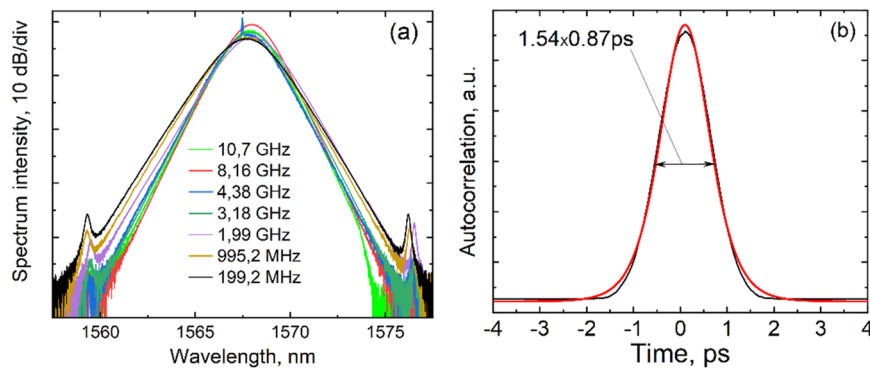


FIG. 9. Typical optical spectra recorded with the soliton fiber laser operating in the DHML regimes at different PRRs (a) and the autocorrelation function of the optical pulses measured with the laser operating in DHML (black) at ~ 2500 MHz and its fitting measured by using the sech function.

equal to the fundamental frequency, f_0 , are deeply suppressed. At low laser frequencies, the intermediate laser states are stable and an accurate PC adjustment can still be used to control the mutual precessions of the elementary pulse sequences to an extent. However, at higher frequencies, the system alone tends to equalize the spacing between the pulses in the laser cavity slowly approaching the robust DHML operation (Visualization 4). The DHML operation with a PRR of up to ~ 12 GHz is achievable in this way.

To complete the picture, several important measurements have been performed with the soliton laser. Figure 9(a) shows the laser optical spectra recorded with the laser operating in the DHML regime. The optical spectrum FWHM width is ~ 3 nm and does not change significantly with PRR. The Kelly sidebands indicate that the fiber laser operates in the soliton regime. We have checked that the precise adjustment of the HML laser to OAR has a minor effect on the recorded optical spectrum. Figure 9(b) shows the pulse autocorrelation functions recorded with laser operating DHML and its fitting recorded by using the sech function. The FWHM pulse duration, estimated to be ~ 870 fs by fitting the data to a hyperbolic secant function (with an autocorrelation function width of ~ 1.34 ps), remains consistent across different laser operation regimes. In general, the DHML laser operation shows good long-term stability. We have run the laser continuously over 10 h without observing any pulse train degradation.

IV. DISCUSSION

The HML is based on multi-pulsing due to the interplay between the laser cavities' bandwidth constraints and the energy quantization for mode-locked pulses. The gain bandwidth of the cavity limits the growth of the mode-locked spectral bandwidth with increased pump power. A single pulse splits into multiple pulses to overcome this constraint. Thereby, the energy is distributed between the pulses, and the bandwidths remain within the gain bandwidth window.⁵⁰ This splitting may be accompanied by the electrostriction effect in the form of excitation of the GAWBS (radial R_{0m} and torsional-radial TR_{2m}) acoustic modes, which could improve the pulsed laser operation. However, the strength of this effect depends on the fiber laser design and alignment.

We have found that the laser shown in Fig. 1, without OAR adjustment, operates as a traditional HML laser, enabling PRR tuning up to 6 GHz. In this operation, the primary mechanism equalizing the soliton spacing in the laser cavity is not the OAR but the repulsive forces between the pulses provided by the GDR processes.¹⁹ Simultaneously, aligning one of the laser harmonics to the OAR (in the experiment, the 15th laser harmonic at $f_{res} = 15 \times 13.27$ MHz has been locked to the TR_{29} mode at 199 MHz) significantly changes the laser operation to that referred as DHML here, enabling the PRR tuning range extended up to ~ 12 GHz. In the DHML regime, the laser can operate at different harmonics of the selected OAR frequency f_{res} consistently delivering robust pulse sequences with enhanced timing jitter, RIN, SSL, and improved long-term stability. It is noteworthy that traditional HML lasers stabilized through the OAR operate with the only PRR equal to the OAR frequency f_{res} .^{37–39} In those experiments, the laser cavity consists of a photonic crystal fiber that maintains a strong OAR throughout the cavity length. This feature makes the HML operation resilient to pump power variations, allowing the pump power to control the laser optical bandwidth and pulse duration but not the PRR. In contrast, the DHML operation is observed with a soliton laser spliced from a standard optical fiber with a 50 cm segment of unjacketed fiber preadjusted for narrow-band ($\Delta f_a \sim 80$ kHz) GAWBS resonance. As the pump power increases, the laser falls to the HML operation with the PRR equal to the OAR frequency f_{res} and then doubles, triples, or further multiplexes the initial PRR.

While a detailed theoretical description of DHML is in progress, we can offer some insight into the possible mechanisms underlying the transition of pulse spacing, especially its relation to optoacoustic coupling. Our current understanding of the DHML is consistent with our experimental observations and could be encapsulated in the following statements:

1. Laser radiation circulating in a properly adjusted cavity (with the fundamental frequency f_0) excites permanent vibrations at the frequency $f_{res} = N_{res}f_0$ in the unjacketed fiber segment.⁴⁵ Given that the GAWBS resonance at $f_a \sim f_{res}$ is narrow-band [$\Delta f_a \sim 80$ kHz, as shown in Fig. 3(a)], the unjacketed fiber segment inserted into the laser cavity acts as a local phase modulator driven by a harmonic signal at f_{res} . This modulation

influences the radiation circulating in the laser cavity by establishing effective phase matching (and energy exchange) between all pairs of optical cavity modes whose eigenfrequencies are spaced by f_{res} . As a result, the laser intensity circulating inside the cavity exhibits RF spectra comprising only modes spaced by f_{res} , while other modes spaced by f_0 are suppressed due to the Vernier effect (see Figs. 6–8). This RF spectrum corresponds to a pure periodic laser intensity signal with the period $T_{res} \sim 1/f_{res}$. It means that the laser intensity signal, originally determined in one OAR period (in the running frame), is simply repeated $N_{res} = f_{res}/f_0$ times over the cavity round-trip time $T_0 \sim 1/f_0$. This fundamental property of the reported laser operation has been observed in all the presented experiments. In particular, it is evident in Visualizations 1–4. Paused at any moment, these visualizations always highlight the periodicity of the laser intensity with the period T_{res} , which is crucial for the permanent support of the OAR.

2. We believe that the equidistant intensity modes spaced by f_{res} play the same role in the DHML mechanism as the modes spaced by f_0 play in the HML. Upon reaching the soliton generation threshold, these modes, in cooperation with the NPE, undergo mode-locking at f_{res} , leading to the formation of a single soliton pulse linked to one OAR period (in the running frame). For the cavity round-trip time $T_0 \sim 1/f_0$, this single soliton is repeated N_{res} times, resulting in N_{res} soliton pulses evenly distributed over the laser cavity. Specifically, for this HML laser operation, the OAR provides an additional means to stabilize the soliton train at f_{res} .³⁵ When the offset between the selected laser cavity harmonic and acoustic mode frequencies $\delta < 0$, the periodic refractive index modulation $\Delta n(t)$ governed by the soliton train through the OAR traps the individual soliton position within the $\Delta n(t)$ period. The second-order term in the Taylor series for $\Delta n(t)$ around the soliton equilibrium position is responsible for this process. Acting together with the cavity's group-velocity dispersion, it creates a "trapping potential well" for the soliton timing that restores the soliton to its initial equilibrium time after it is perturbed. Analyzing this formalism further, one can conclude that the steepness of the potential well trapping the soliton within the $\Delta n(t)$ period depends on $-\delta$ and reaches its maximum at $-\delta \sim 0.5$, enabling maximal laser stability to external perturbations. In relation to our experiment, we can assign $-\delta \sim 0.5$ to the left experimental point shown in Fig. 3(b), where the stability of the laser operation is strongest. It is reasonable since at this point, the rise of pump power up to 900 mW does not affect the fundamental laser PRR = f_{res} . In contrast, when gradual fiber stretching is applied and $-\delta$ increases, the steepness of the potential well is reduced as $1/\sqrt{\delta^2 + 1}$, resulting in a decrease in the OAR trapping strength. Therefore, in the next experimental points shown in Fig. 3(b), the same increase in pump power causes doubling, tripling, and further multiplexing of the soliton pulse within the same $\Delta n(t)$ period. This soliton multiplexing reaches a maximum value of 60 at $-\delta$ estimated to be 4.2, where the effect of the OAR stabilization is weakest.
3. In their transition to DHML with an increase in pump power, a single pulse circulating within one $\Delta n(t)$ period splits into

multiple soliton pulses as a result of energy quantization (similar to HML lasers). In this step, an interplay between different soliton interactions (e.g., through dispersive waves, GDR, and OAR) causes permanent wandering of individual solitons within the linked OAR period (see Visualization 3). Notably, the system maintains its periodicity at f_{res} all the time, and any current distribution of pulses within one OAR period replicates N_{res} times over the cavity round-trip time T_0 . This means that the pulse sequence circulating in the ring cavity consists of many overlapped but rather independent pulse sequences, all with the PRR = f_{res} . The RF spectrum shown in Figs. 8(b) and 8(e) exhibits features specific to a superposition of many regular pulse sequences, each randomly shifted relative to the others.

4. To achieve DHML operation with all circulating pulses, the delays between these elementary sequences must be somehow equalized. We believe that the GDR mechanism, operating against the OAR-induced trapping, is responsible for this process. In this cooperation, the GDR mechanism provides repulsion between adjacent soliton pulses, while the trapping effect attempts to collect all pulses belonging to the same $\Delta n(t)$ period in a single equilibrium point. The OAR-induced trapping prevents pulse splitting but becomes less significant when the GDR forces the pulses to move apart. Finally, the trapping effect is completely eliminated in the DHML regime because the equidistant pulses at the f_{res} harmonics do not contribute to the OAR at f_{res} .^{34,35} The competition between the GDR and OAR trapping is controllable by the pump power and fiber stretching (i.e., δ) as they govern the strengths of the first and second mechanisms, respectively. As soon as the threshold pump power level is achieved, the GDR forces the pulses to split and move apart and the OAR trapping effect vanishes, thus facilitating the laser's transition to the DHML regime. This understanding is confirmed by comparison of the RF laser spectra shown in Fig. 8. The pronounced peak at f_{res} and supermodes spaced by f_{res} , both resulting from narrow-band acoustic vibrations, dominate the spectra recorded in the intermediate laser regimes [Figs. 8(b) and 8(e)]. However, they are absent in the laser spectra recorded in the established DHML regime [Figs. 8(a), 8(c), 8(d), and 8(f)] because the vibrations are supported at noise level only.
5. We also believe that the enhanced laser stability demonstrated in our experiments in the DHML regime is provided by the GDR repulsion mechanism operating together with the OAR. In this cooperation, the GDR strengthens the repulsion between adjacent soliton pulses, forcing their equalization within one OAR period. In turn, the OAR enables long-lived acoustic vibrations at f_{res} that impose strong periodicity on the laser intensity, thus enabling long-range interaction between the pulses relating to different OAR periods. This interaction transforms the repulsion between the nearest pulses into repulsion between the elementary pulse sequences superposing the pulse train and thus multiplying the local forces provided by the GDR. In this way, the system equilibrates itself through its tendency to stabilize DHML, involving a mechanism somewhat similar to the long-range Casimir-like interactions^{52,53} often responsible for the formation of stable dynamical patterns within ultrafast lasers.

V. CONCLUSION

In conclusion, we have explored a novel high-frequency HML regime distinct from both traditional HML and previously reported HML enhanced by OAR. The observed laser behavior can be interpreted as a double HML. The initial HML process governed by OAR forms a stable elementary pulse sequence at the OAR frequency f_{res} . This OAR also guides the creation of two, three, or more similar elementary pulse sequences at the OAR frequency superposed in the fiber cavity at higher pump power levels. Subsequently, the GDR mechanism enhanced by the OAR equilibration process takes over to equalize soliton spacing within the laser cavity, thus resulting in the double HML of the laser and ensuring a low pulse timing jitter, relative intensity noise (RIN), and high SSL at gigahertz repetition rates. Our findings provide crucial insights into the 12 GHz HML laser operation at ~ 900 cavity harmonics that are enabled and stabilized through the OAR in the standard optical fiber, vital for HML laser design and optimization.

SUPPLEMENTARY MATERIAL

See the [supplementary material](#) for Visualizations 1–4.

ACKNOWLEDGMENTS

This study was supported by the Russian Science Foundation (Grant No. 23-79-30017).

AUTHOR DECLARATIONS

Conflict of Interest

The authors have no conflicts to disclose.

Author Contributions

V. A. Ribenek: Formal analysis (equal); Investigation (equal); Validation (equal); Visualization (equal); Writing – original draft (equal). **P. A. Itrin:** Data curation (equal); Investigation (equal); Methodology (equal); Software (equal); Validation (equal); Visualization (equal); Writing – original draft (equal). **D. A. Korobko:** Conceptualization (equal); Formal analysis (equal); Funding acquisition (equal); Investigation (equal); Methodology (equal); Supervision (equal); Validation (equal); Visualization (equal); Writing – original draft (equal). **A. A. Fotiadi:** Conceptualization (equal); Investigation (equal); Methodology (equal); Supervision (equal); Validation (equal); Visualization (equal); Writing – original draft (equal); Writing – review & editing (equal).

DATA AVAILABILITY

Data underlying the results presented in this paper are not publicly available at this time but may be obtained from the authors upon reasonable request.

REFERENCES

¹O. Kovalchuk, S. Lee, H. Moon, A. M. Armani, and Y.-W. Song, “Non-planar graphene directly synthesized on intracavity optical microresonators for GHz repetition rate mode-locked lasers,” *npj 2D Mater. Appl.* **8**, 3 (2024).

²A. Aadhi, I. Alamgir, L. Di Lauro, B. Fischer, N. Perron, P. Dmitriev, C. Mazoukh, P. Roztocky, C. Rimoldi, M. Chemnitz, A. Eshaghi, E. A. Viktorov, A. V. Kovalev, B. E. Little, S. T. Chu, D. J. Moss, and R. Morandotti, “Mode-locked laser with multiple timescales in a microresonator-based nested cavity,” *APL Photonics* **9**, 031302 (2024).

³A. Cutrona, M. Rowley, A. Bendahmane, V. Ceconi, L. Peters, L. Olivieri, B. E. Little, S. T. Chu, S. Stivala, R. Morandotti, D. J. Moss, J. S. Toterogongora, M. Peccianti, and A. Pasquazi, “Stability of laser cavity-solitons for metrological applications,” *Appl. Phys. Lett.* **122**, 121104 (2023).

⁴S. Huang, Y. Liu, H. Liu, Y. Sun, R. Xia, W. Ni, Y. Luo, L. Yan, H. Liu, Q. Sun, P. P. Shum, and X. Tang, “Isomeric dynamics of multi-soliton molecules in passively mode-locked fiber lasers,” *APL Photonics* **8**, 036105 (2023).

⁵U. Keller, “Recent developments in compact ultrafast lasers,” *Nature* **424**, 831–838 (2003).

⁶H. Kalaycıoğlu, P. Elahi, Ö. Akcaalan, and F. O. Ilday, “High-repetition-rate ultrafast fiber lasers for material processing,” *IEEE J. Sel. Top. Quantum Electron.* **24**, 1–12 (2018).

⁷M. E. Fermann, A. Galvanauskas, and G. Sucha, *Ultrafast Lasers: Technology and Applications* (Taylor & Francis, 2003).

⁸M. E. Fermann and I. Hartl, “Ultrafast fibre lasers,” *Nat. Photonics* **7**, 868–874 (2013).

⁹A. B. Grudinin and S. Gray, “Passive harmonic mode locking in soliton fiber lasers,” *J. Opt. Soc. Am. B* **14**, 144 (1997).

¹⁰X. Liu and M. Pang, “Revealing the buildup dynamics of harmonic mode-locking states in ultrafast lasers,” *Laser Photonics Rev.* **13**, 1800333 (2019).

¹¹J. N. Kutz, B. C. Collings, K. Bergman, and W. H. Knox, “Stabilized pulse spacing in soliton lasers due to gain depletion and recovery,” *IEEE J. Quantum Electron.* **34**, 1749–1757 (1998).

¹²D. A. Korobko, O. G. Okhotnikov, and I. O. Zolotovskii, “Long-range soliton interactions through gain-absorption depletion and recovery,” *Opt. Lett.* **40**, 2862–2865 (2015).

¹³E. M. Dianov, A. V. Luchnikov, A. N. Pilipetskii, and A. N. Starodumov, “Electrostriction mechanism of soliton interaction in optical fibers,” *Opt. Lett.* **15**, 314–316 (1990).

¹⁴J. K. Jang, M. Erkintalo, S. G. Murdoch, and S. Coen, “Ultraweak long-range interactions of solitons observed over astronomical distances,” *Nat. Photonics* **7**, 657 (2013).

¹⁵A. N. Pilipetskii, E. A. Golovchenko, and C. R. Menyuk, “Acoustic effect in passively mode-locked fiber ring lasers,” *Opt. Lett.* **20**, 907–909 (1995).

¹⁶E. M. Dianov, A. V. Luchnikov, A. N. Pilipetskii, and A. M. Prokhorov, “Long-range interaction of picosecond solitons through excitation of acoustic waves in optical fibers,” *Appl. Phys. B: Photophys. Laser Chem.* **54**, 175–180 (1992).

¹⁷W. H. Loh, V. V. Afanasjev, D. N. Payne, and A. B. Grudinin, “Soliton interaction in the presence of a weak nonsoliton component,” *Opt. Lett.* **19**, 698–700 (1994).

¹⁸V. A. Ribenek, D. A. Korobko, A. A. Fotiadi, and J. R. Taylor, “Supermode noise mitigation and repetition rate control in a harmonic mode-locked fiber laser implemented through the pulse train interaction with co-lased CW radiation,” *Opt. Lett.* **47**, 5236–5239 (2022).

¹⁹D. A. Korobko, V. A. Ribenek, D. A. Stoliarov, P. Mégret, and A. A. Fotiadi, “Resonantly induced mitigation of supermode noise in a harmonically mode-locked fiber laser: Revealing the underlying mechanisms,” *Opt. Express* **30**, 17243–17258 (2022).

²⁰D. A. Korobko, V. A. Ribenek, P. A. Itrin, D. A. Stoliarov, and A. A. Fotiadi, “Polarization maintaining harmonically mode-locked fiber laser with suppressed supermode noise due to continuous wave injection,” *Opt. Laser Technol.* **162**, 109284 (2023).

²¹S. Gray, A. B. Grudinin, W. H. Loh, and D. N. Payne, “Femtosecond harmonically mode-locked fiber laser with time jitter below 1 ps,” *Opt. Lett.* **20**, 189–191 (1995).

²²D. Korobko, D. Stoliarov, P. Itrin, V. Ribenek, M. Odnoblyudov, A. Petrov, and R. Gumenyuk, “Stabilization of a harmonic mode-locking by shifting the carrier frequency,” *J. Lightwave Technol.* **39**, 2980–2987 (2021).

²³R. Gumenyuk, D. Korobko, and I. Zolotovskii, “Stabilization of passive harmonic mode locking in a fiber ring laser,” *Opt. Lett.* **45**, 184–187 (2020).

- ²⁴V. A. Ribenek, D. A. Stoliarov, D. A. Korobko, and A. A. Fotiadi, "Mitigation of the supermode noise in a harmonically mode-locked ring fiber laser using optical injection," *Opt. Lett.* **46**, 5747–5750 (2021).
- ²⁵Y. Wang, F. Leo, J. Fatome, M. Erkintalo, S. G. Murdoch, and S. Coen, "Universal mechanism for the binding of temporal cavity solitons," *Optica* **4**, 855–863 (2017).
- ²⁶S. Sergeyev, H. Khashi, N. Tarasov, Y. Loiko, and S. Kolpakov, "Vector-resonance-multimode instability," *Phys. Rev. Lett.* **118**, 033904 (2017).
- ²⁷S. Sergeyev, S. Kolpakov, and Y. Loika, "Vector harmonic mode-locking by acoustic resonance," *Photonics Res.* **9**, 1432–1438 (2021).
- ²⁸M. Sumetsky, "Optical bottle versus acoustic bottle and antibottle resonators," *Opt. Lett.* **42**, 923–926 (2017).
- ²⁹M. Sumetsky, "Optical frequency combs generated mechanically," *Opt. Lett.* **42**, 3197–3200 (2017).
- ³⁰R. Si Fodil, F. Amrani, C. Yang, A. Kellou, and P. Grelu, "Adjustable high-repetition-rate pulse trains in a passively-mode-locked fiber laser," *Phys. Rev. A* **94**, 013813 (2016).
- ³¹M. Peccianti, A. Pasquazi, Y. Park, B. E. Little, S. T. Chu, D. J. Moss, and R. Morandotti, "Demonstration of a stable ultrafast laser based on a nonlinear microcavity," *Nat. Commun.* **3**, 765 (2012).
- ³²V. Dvoyrin and M. Sumetsky, "Bottle microresonator broadband and low-repetition-rate frequency comb generator," *Opt. Lett.* **41**, 5547–5550 (2016).
- ³³J. Lee and J. H. Lee, "Experimental investigation of the cavity modulation frequency detuning effect in an active harmonically mode-locked fiber laser," *J. Opt. Soc. Am. B* **30**, 1479 (2013).
- ³⁴M. Pang, W. He, X. Jiang, and P. S. J. Russell, "All-optical bit storage in a fibre laser by optomechanically bound states of solitons," *Nat. Photonics* **10**, 454–458 (2016).
- ³⁵W. He, M. Pang, D. H. Yeh, J. Huang, C. R. Menyuk, and P. S. J. Russell, "Formation of optical supramolecular structures in a fibre laser by tailoring long-range soliton interactions," *Nat. Commun.* **10**, 5756 (2019).
- ³⁶D.-H. Yeh, W. He, M. Pang, X. Jiang, G. Wong, and P. S. J. Russell, "Pulse-repetition-rate tuning of a harmonically mode-locked fiber laser using a tapered photonic crystal fiber," *Opt. Lett.* **44**, 1580–1583 (2019).
- ³⁷M. S. Kang, N. Y. Joly, and P. S. Russell, "Passive mode-locking of fiber ring laser at the 337th harmonic using gigahertz acoustic core resonances," *Opt. Lett.* **38**, 561–563 (2013).
- ³⁸M. Pang, X. Jiang, W. He, G. K. L. Wong, G. Onishchukov, N. Y. Joly, G. Ahmed, C. R. Menyuk, and P. S. J. Russell, "Stable subpicosecond soliton fiber laser passively mode-locked by gigahertz acoustic resonance in photonic crystal fiber core," *Optica* **2**, 339 (2015).
- ³⁹W. He, M. Pang, D. H. Yeh, and P. S. J. Russell, "Optoacoustic mode-locking based on micro-core photonic crystal fibre," in *2021 26th Microoptics Conference (MOC)* (IEEE, 2021), pp. 1–2.
- ⁴⁰R. M. Shelby, M. D. Levenson, and P. W. Bayer, "Guided acoustic-wave Brillouin scattering," *Phys. Rev. B* **31**, 5244–5252 (1985).
- ⁴¹A. J. Poustie, "Bandwidth and mode intensities of guided acoustic-wave Brillouin scattering in optical fibers," *J. Opt. Soc. Am. B* **10**, 691–696 (1993).
- ⁴²F. Yaman, K. Nakamura, E. Mateo, S. Fujisawa, H. G. Batshon, T. Inoue, Y. Inada, and T. Wang, "Guided acoustic Brillouin scattering measurements in optical communication fibers," *Opt. Express* **29**, 17628–17668 (2021).
- ⁴³H. J. Khashi, S. V. Sergeyev, M. Al-Araimi, A. Rozhin, D. Korobko, and A. Fotiadi, "High-frequency vector harmonic mode locking driven by acoustic resonances," *Opt. Lett.* **44**, 5112–5115 (2019).
- ⁴⁴Y. Liu, Y. Ning, Y. Gu, P. Chen, K. Jiang, L. Wang, Y. You, W. He, and X. Chou, "Ultra-narrow linewidth dual-cavity opto-mechanical microwave oscillator based on radial guided acoustic modes of single-mode fiber," *Appl. Phys. Lett.* **122**, 041107 (2023).
- ⁴⁵A. J. Poustie, "Guided acoustic-wave Brillouin scattering with optical pulses," *Opt. Lett.* **17**, 574–576 (1992).
- ⁴⁶R. Shelby, M. Levenson, and P. Bayer, "Resolved forward Brillouin scattering in optical fibers," *Phys. Rev. Lett.* **54**, 939 (1985).
- ⁴⁷D. M. Chow, Z. Yang, M. A. Soto, and L. Thévenaz, "Distributed forward Brillouin sensor based on local light phase recovery," *Nat. Commun.* **9**, 2990 (2018).
- ⁴⁸L. A. Sánchez, A. Díez, J. L. Cruz, and M. V. Andrés, "Recent advances in forward Brillouin scattering: Sensor applications," *Sensors* **23**, 318 (2023).
- ⁴⁹V. A. Ribenek, D. A. Stoliarov, D. A. Korobko, and A. A. Fotiadi, "Pulse repetition rate tuning of a harmonically mode-locked ring fiber laser using resonant optical injection," *Opt. Lett.* **46**, 5687–5690 (2021).
- ⁵⁰D. Y. Tang, L. M. Zhao, B. Zhao, and A. Q. Liu, "Mechanism of multisoliton formation and soliton energy quantization in passively mode-locked fiber lasers," *Phys. Rev. A* **72**, 043816 (2005).
- ⁵¹F. Rana, H. L. T. Lee, R. J. Ram, M. E. Grein, L. A. Jiang, E. P. Ippen, and H. A. Haus, "Characterization of the noise and correlations in harmonically mode-locked lasers," *J. Opt. Soc. Am. B* **19**, 2609–2621 (2002).
- ⁵²R. Weill, A. Bekker, V. Smulakovsky, B. Fischer, and O. Gat, "Noise-mediated Casimir-like pulse interaction mechanism in lasers," *Optica* **3**, 189 (2016).
- ⁵³K. Sulimany, O. Lib, G. Masri, A. Klein, M. Fridman, P. Grelu, O. Gat, and H. Steinberg, "Bidirectional soliton rain dynamics induced by Casimir-like interactions in a graphene mode-locked fiber laser," *Phys. Rev. Lett.* **121**, 133902 (2018).